Foehn-induced effects on local dust pollution, frontal clouds and solar radiation in the Dead Sea valley

Pavel Kishcha[1], Boris Starobinets[1], Amit Savir[2], Pinhas Alpert[1] and Michael Kaplan[3]

[1]*School of Geosciences, Tel-Aviv University, 69978 Tel-Aviv, Israel*

[2]*Israel Meteorological Service, Israel*

[3]*Desert Research Institute, USA*

Meteorology and Atmospheric Physics, doi:10.1007/s00703-017-0521-1.

Abstract

Despite the long history of investigation of foehn phenomena, there are few studies of the influence of foehn winds on air pollution and none in the Dead Sea valley. For the first time the foehn phenomenon and its effects on local dust pollution, frontal cloudiness and surface solar radiation were analyzed in the Dead Sea valley, as it occurred on 22 March 2013. This was carried out using both numerical simulations and observations. The foehn winds intensified local dust emissions, while the foehn-induced temperature inversion trapped dust particles beneath this inversion. These two factors caused extreme surface dust concentration in the western Dead Sea valley. The dust pollution was transported by west winds eastward, to the central Dead Sea valley, where the speed of these winds sharply decreased. The transported dust was captured by the ascending airflow contributing to the maximum aerosol optical depth (AOD) over the central Dead Sea valley. On the day under study, the maximum surface dust concentration did not coincide with the maximum AOD: this being one of the specific effects of the foehn phenomenon on dust pollution in the Dead Sea valley. Radar data showed a passage of frontal cloudiness through the area of the Dead Sea valley leading to a sharp drop in noon solar radiation. The descending airflow over the downwind side of the Judean Mountains led to the formation of a cloud-free band followed by only the partial recovery of solar radiation because of the extreme dust pollution caused by foehn winds.

1 Introduction

The Dead Sea valley is a unique place because the coastal area of the extremely saline Dead Sea is an area of dry land with the lowest elevation on Earth (-420 m ASL). (Hereafter all heights are given in meters above sea level). This valley is flanked by mountains of ~1000 m height: by the Moab Mountains to the east and by the Judean Mountains to the west. Both the Judean Mts. and the Moab Mts. exhibit a north-south alignment (Fig. 1). Strong west winds, blowing perpendicularly to the Judean Mts., can cause the foehn phenomenon in the Dead Sea valley.

Foehn is a generic term for a downslope wind that is strong, warm, and dry (Brinkmann 1971; Richner and Hächler 2013 and references therein). The term foehn originates in the Alpine area, where, during a foehn phenomenon in a valley, a rise in temperature, a drop in relative humidity, and the onset of high winds in a constant wind direction all occur within minutes. Foehn winds occur downstream of most major mountain ridges in the world (Drechsel and Mayr 2008; Nkemdirim and Leggat 1978; Norte 2015; Takane and Kusaka 2011). These winds sometimes bear their own regional names like “chinook” east of the North American Rockies and “zonda” downstream of the South American Andes. Despite the fact that the foehn phenomenon has been investigated for a long time, there are few studies of the influence of foehn winds on air pollution (Gohm et al. 2009; Li et al. 2015; McGowan et al. 1996, 2002).

To our knowledge, the foehn phenomenon has not been studied over the unique territory of the Dead Sea valley. The current study was aimed at investigating the formation of the foehn phenomenon over the Judean Mountains, as it occurred on 22 March 2013. Our analysis of this event was carried out using numerical simulations and in situ observations at meteorological stations located across the mountain ridge. Particular attention was given to the effect of the foehn phenomenon on local dust pollution, frontal clouds and incoming solar radiation.

The foehn phenomenon under investigation in the current study is not the typical foehn phenomenon of the European Alps, where saturated adiabatic ascent on the upwind side of the high mountain ridge is accompanied by precipitation. In our case, the minimum temperature at the top of the Judean Mts. on the date under study was too high to form precipitation reaching the surface on the upwind side. The other characteristics of the foehn phenomenon under consideration, such as an increase in wind speed and its gustiness on the downwind side of the Judean Mts., as well as a rise in temperature, and a decrease in relative humidity were similar to those in the typical Alpine foehn.

The current study was carried out in the framework of the DESERVE (DEad SEa Research Venue) project started in 2013 (www.deserve-vi.net). This project aims at studying coupled lithospheric, hydrological, and atmospheric processes in the Dead Sea region.

2 Methodology

To study the foehn phenomenon on the downwind side of the Judean Mts. and in the Dead Sea valley, we used available meteorological measurements and numerical simulations as described below.

2.1 Measurements

The dataset consists of in situ meteorological measurements from a latitudinal chain of eight monitoring stations, located across the Judean Mountains ridge and in the Dead Sea (Fig. 1). This chain includes three sites at the upwind side of the Judean Mts. (Nizzan, Hafaz Hayyim, Nativ Halamed Hay), two sites near its top (Rosh Zurim and Jerusalem), two sites at its downwind side (Maale Adumim, Matzukei Dargot) and a hydrometeorological buoy, anchored in the Dead Sea (Table 1). These seven monitoring meteorological sites are operated by the Israel Meteorological Service. The dataset of their observations includes 10-minute standard meteorological parameters such as air temperature, air pressure, relative humidity, wind speed and direction. The Dead Sea buoy is operated by the Israel Oceanographic and Limnological Research and located at approximately 5 km offshore (Fig. 1). The dataset of buoy observations includes 20-minute air measurements such as temperature, pressure, relative humidity, wind speed and direction, as well as incoming solar radiation. These data were collected on a regular basis at the buoy at 3 m height above the sea surface.

Cloud heights and precipitation rate were analyzed using radar measurements. This radar (C-band with the 5-cm wavelength) is operated by the Israel Meteorological Service and located at Bet Dagan, near the Mediterranean coast (Fig. 1). Variations of incoming solar radiation (global radiation) were investigated using pyranometer measurements collected at the Negba station, located near the Mediterranean coast, and at the above-mentioned hydrometeorological buoy in the Dead Sea (Fig. 1).

2.2 Modeling

The online-coupled COSMO-ART model simulations of dust, with 3-km horizontal grid spacing, were carried out from 21 March, 1200 UTC, to 23 March, 1200 UTC. This model is based on the COSMO (**Co**nsortium for **S**mall-scale **Mo**delling) meteorological model (Baldauf et al. 2011) used in several European countries for numerical weather prediction. COSMO-ART includes the ART (**A**erosols and **R**eactive **T**race gases) module to describe the 3-D distribution of dust aerosol particles (Vogel et al. 2009). COSMO-ART describes emissions, transport, and deposition of desert dust. Mineral dust aerosol is represented by prognostic mass and number densities of three overlapping log-normally distributed modes. Properties of soil (surface roughness, particle size distribution) and environmental conditions (friction velocity, soil moisture) define the dust productive area. The data set of soil properties by Marticorena et al. (1997) and Callot et al. (2000) is used. The friction velocity, describing the impact of the turbulent impulse energy onto the soil surface, is the key parameter for dust production in COSMO-ART. Dust is produced when the friction velocity exceeds the threshold friction velocity. In COSMO-ART, the threshold friction velocity is determined by factors taking into account soil-water content and surface roughness (Vogel et al. 2006). In the current study, we investigated local dust pollution from sources in the area of the Dead Sea valley covering the domain (within the red box shown in Fig. 2) with its western boundary at the top of the Judean Mts. The model dust simulation started with a dust-free atmosphere (the cold start with respect to dust).

Meteorological parameters are obtained from COSMO-ART meteorological simulations over the three nested domains (Fig. 2): a) the large domain with 0.25° horizontal grid spacing and 40 vertical layers up to 22 km height; b) the middle domain with 0.0650^{o} (~7 km) horizontal grid spacing including the Eastern Mediterranean; and c) the small domain with 0.025° (~3 km) horizontal grid spacing including the Dead Sea valley and surrounding areas. The large domain received its initial and boundary conditions from the global model GME, from the German Weather Service (DWD). The middle domain used its initial and boundary conditions from the coarse-resolution simulation over the large domain, while the small domain used its initial and boundary conditions from the middle domain.

3 The foehn phenomenon in the Dead Sea valley on March 22, 2013

On March 22, 2013, a low-pressure system was observed over the Eastern Mediterranean with its center near Cyprus (hereafter the Cyprus low). It created favorable conditions for dust uplifting from the Eastern Sahara and transport by south-west winds into the Eastern Mediterranean. The following shift of this Cyprus low eastward was accompanied by increasing southwesterly to westerly winds over Israel. At 1200 UTC, this Cyprus low was characterized by sea level pressure below 995 hPa at its center near Cyprus, as illustrated by the spatial distribution of sea level pressure based on the NASA MERRA reanalysis data (Fig. 3a). The passage of the Cyprus low with its frontal system over Israel toward the Dead Sea valley was accompanied by frontal cloudiness and by the development of a foehn phenomenon. Moreover, dust pollution was transported over Israel, as illustrated by the operational DREAM/TAU (**D**ust **Re**gional **M**odel running at **T**el **A**viv **U**niversity) dust model data (Fig. 3b). A spacial-temporal distribution of the dust pollution on the date under consideration was discussed in our previous study by Kishcha et al. (2016).

3.1 Variations of horizontal wind

In order to demonstrate the development of the foehn phenomenon on the downwind side of the Judean Mts. during the Cyprus low passage over these mountains, Fig. 4 represents diurnal variations of measured wind speed and wind direction in Jerusalem (810 m), Matzukei Dargot (20 m) and at the Dead Sea buoy (-420 m). One can see that, in Jerusalem, from 0930 UTC to 1030 UTC the wind changed its direction from south-west to west, which was accompanied by an increase in 10-minute average wind speed from 5 m/s to 10 m/s, with measured wind gusts up to 20 m/s. This strong wind, perpendicular to the Judean Mountains ridge, created favourable conditions for the formation of a foehn phenomenon on the lee side of the ridge. After a 90-minute delay with respect to the wind increase in Jerusalem, a sharp increase in 10-min average wind speed from ~2 m/s to 20 m/s occurred in Matzukei Dargot, from 1000 UTC to 1200 UTC (Fig. 4). Wind gusts up to 28 m/s were detected there. One hour later with respect to the wind increase in Matzukei Dragot, the Dead Sea buoy also showed an increase in 20-minute average wind speed from 2 m/s to 10 m/s from 1100 UTC to 1300 UTC. The detected wind gusts were as high as 20 m/s. The above-mentioned measured strong increase in wind speed and gustiness indicated the onset of a foehn phenomenon (Drechsel and Mayr, 2008).

Figure 5 represents changes in the U-component of the near surface wind, blowing across the Judean Mts. ridge, within the west-east cross-section at 31.6^{o}C (where the height of this ridge is maximal). At 1000 UTC, under south-west winds, the measured U-component of the near surface wind on the upwind side of ~7 m/s exceeded that on the downwind side, which was characterized by wind speed of less than 5 m/s. One hour later, after the wind changed direction from south-west to west, the measured wind speed on the downwind side started increasing. Then, at 1200 UTC, a local maximum in measured wind speed occurred on the downwind side. At 1300 UTC, this maximum on the downwind side of the Judean Mts. was double the wind speed on the upwind side. After 1200 UTC, the speed of the U-component sharply decreased over the central Dead Sea valley in the area of the ascending airflow (see Section 3.2).

Note that, at 1100 - 1300 UTC, the modeled near-surface U-component overestimated measurements by about 5 m/s on the upwind side (Fig. 5). Despite this model overestimation, model data showed that, as a result of the foehn phenomenon, the maximum in U-component of horizontal wind on the downwind side was double the wind speed on the upwind side. In this respect, the simulated U-components of near-surface wind were consistent with the above-mentioned wind measurements.

In order to demonstrate wind variations at different altitudes over the Judean Mts. and over the Dead Sea valley, Fig. 6 shows a vertical distribution of modeled U-component of horizontal wind within the west-east cross-section (at 31.6^{o}N) at various times. Before 1200 UTC only moderate wind is simulated. At 1200 UTC, wind speed increased sharply when south-west winds were replaced by west winds in the upwind side of the Judean Mts. The most intense west winds of over 30 m/s along the downwind side of the Judean Mts. occurred at 1300 UTC (Fig. 6). These winds were twice as strong as the winds on the upwind side of the ridge. These winds activated local dust sources, contributing to extreme dust concentration observed in the Dead Sea valley on March 22, 2016 (Section 3.3).

3.2 Vertical airflow

To demonstrate the effect of the strong west winds on vertical airflow over the Judean Mts. and over the Dead Sea valley, we analyzed west-east vertical cross-sections of modelled vertical wind at latitude 31.6^{o}N, at various times. Fig. 7 shows that before 1200 UTC only some moderate vertical motion was simulated, including ascending airflow on the upwind side and descending airflow on the downwind side. At 1200 UTC, the vertical motion increased significantly after a sharp increase in the west wind. The most intense descending airflow on the lee side of the Judean Mts. and ascending airflow in the Dead Sea valley occurred at 1300 UTC. As estimated, on the lee side of the Judean Mountains, a maximum downward velocity exceeded 1.5 m/s. In the centre of the Dead Sea valley, a maximum upward velocity of over 2 m/s was obtained (Fig. 7).

The distribution of potential temperature at 1300 UTC showed that isentropes were parallel to the downwind slope of the Judean Mts. (Fig. 7). Under low relative humidity (~20%, see Section 3.4), airflow on the lee side was adiabatic. For adiabatic airflow, the isentropes are a good indication of streamlines. Indeed, in the area of the descending airflow, the isentropes folded downward, while in the area of the ascending airflow the isentropes folded upward (Fig. 7).

3.3 Temperature inversion as a causal factor of extreme local dust pollution

Both meteorological observations and model data showed that the development of the foehn phenomenon on the downwind side of the Judean Mts. was accompanied by air heating in the Dead Sea valley and air cooling on the top of the Judean Mts. In order to illustrate this result, Fig. 8 (the left panel) represents west-east cross-sections of measured surface temperature over the north of the Dead Sea valley, at various times. It can be seen that, at local noon (1000 UTC), the temperature at the Dead Sea buoy did not exceed the temperature in Rosh Zurim (24^{o}C), at the top of the Judean Mts. One hour later, after the increase in wind speed on the downwind side of the Judean Mts., the temperature at the top of the mountain ridge decreased to 17^{o}C, while that in the valley increased up to 25^{o}C (Fig. 8). So that a temperature difference of 8^{o}C was observed between the top of the mountain ridge and the valley. At 1200 UTC, this temperature difference increased up to 16^{o}C and remained the same at 1300 UTC. This temperature difference was created by the foehn phenomenon: at the top of the Judean Mts. the air became colder because of the adiabatic ascent in the upwind side of the mountains, while in the Dead Sea valley the air became warmer because of the adiabatic descent along the downwind side of the mountains. Note that, before the formation of the foehn phenomenon (at 1000 - 1100 UTC), there is some discrepancy between modeled and observed temperature values (Fig. 8, the left panel). However, after the formation of the foehn phenomenon (at 1200 - 1300 UTC), the correspondence between modeled and observed temperature values was much better.

The model showed that, on the day under consideration, the foehn-induced pronounced temperature inversion (of approximately 400-m thickness) occurred in the western Dead Sea valley at 1300 UTC. This inversion obstructed convection currents and, consequently, trapped local dust particles beneath this inversion (Fig. 9a). As illustrated in Fig. 10a, at longitude 35.4^{o}E of maximum surface dust concentration (Fig. 9c) within the cross-section at 31.6^{o}N, the temperature vertical profile showed that the temperature increased from 20.1^{o}C at 200 m to 22.8^{o}C at 470 m and then remained constant up to 570 m. Our analysis of modeled turbulence kinetic energy (TKE) showed that strong foehn winds of over 20 m/s, blowing along the downwind side of the Judean Mts. at 1300 UTC, were accompanied by intense air turbulence characterized by a strong narrow maximum at longitude 35.4^{o}E (Fig. 9b). This maximum turbulence led to maximum local dust emissions at the same longitude (Fig. 9b). Thus, the model showed that, on the day under consideration, the presence of significant turbulence intensified the saltation mechanism of local dust emissions in the western Dead Sea valley. As known, small mineral dust particles of size less than 10 µm are not lifted directly into the atmosphere by winds because of strong binding forces (Marticorena 2014; Vogel et al. 2006). Instead they are brought into the atmosphere by the following saltation mechanism: particles with a diameter of ~100 µm can be lifted into the atmosphere by winds but fall rapidly back down to the surface due to gravitational forces releasing smaller particles. This saltation mechanism led to the formation of maximum surface dust concentration in the western Dead Sea valley at longitude 35.4^{o}E (Fig. 9c). Moreover, a combined effect of the following two factors: the maximum local dust emissions and the temperature inversion, caused extreme dust concentration beneath the inversion in the western Dead Sea valley, as illustrated by the dust vertical profile shown in Fig. 10a. There was no dust pollution above the inversion (Fig. 10a).

The dust pollution was transported by west winds eastward, to the central Dead Sea valley, where the speed of these winds sharply decreased (Fig. 5, 1300 UTC). As a result, a large part of the transported dust particles was captured by the ascending airflow. This contributed to maximum aerosol optical depth (AOD) at longitude 35.5^{o}E (Fig. 9d). Thus, the model showed that, on the day under consideration, the maximum surface dust concentration did not coincide with the maximum AOD: this being one of the specific effects of the foehn phenomenon on dust pollution in the Dead Sea valley. Figure 10b represents the vertical temperature profile in the central Dead Sea valley, at longitude 35.5^{o}E. It can be seen that there was no temperature inversion there. In the absence of a temperature inversion, the ascending airflow lifted dust particles up to 2-km altitude (Fig. 9a).

3.4 Changes in relative humidity

As the temperature increased in the valley, the relative humidity decreased, while as the temperature decreased on the top of the Judean Mts., the relative humidity increased (Fig. 8, the right panel). This is because relative humidity depends on temperature as well as on moisture content. At 1300 UTC, the measured relative humidity at the top of the mountains reached 85%, which was significantly higher than the relative humidity of 26% in the Dead Sea valley (Fig. 8, the right panel). Note that, before the formation of the foehn phenomenon (1000 - 1100 UTC), there was some discrepancy between modeled and observed relative humidity values (Fig. 8, the right panel). However, after the formation of the foehn phenomenon (1200 - 1300 UTC), a reasonable correspondence was observed between modeled and observed relative humidity.

To demonstrate the effect of the foehn phenomenon on humidity at different altitudes over the Judean Mts. and over the Dead Sea valley, we analyzed west-east vertical cross-sections of modeled relative humidity across the north side of the Dead Sea valley (at 31.6^{o}N), at various times (Fig. 11). While before 1200 UTC only relatively low humidity (mainly less than 40%) was simulated at altitudes below two kilometers over the upwind side of the mountains, it essentially increased when strong west winds (bringing humid air from the Mediterranean Sea) passed through the area. The highest relative humidity exceeding 90% over the upwind side of the Judean Mts. occurred at 1300 UTC. This was caused by the air cooling due to the adiabatic ascending airflow over the upwind side of the mountains. Air heating (due to the descending airflow over the downwind side of the Judean Mts.) was responsible for the significant decrease in relative humidity, below 20% in the Dead Sea valley (Fig. 11).

Furthermore, at 1300 UTC, between 4 - 5 km over the upwind side of the mountains and between 6 - 7 km over the valley, the model showed areas of high relative humidity exceeding 90%. This suggests the possibility for some light rainfall in these two areas. Indeed, according to Fig. 12, radar data showed low precipitation amounts over the upwind side of the Judean Mts. at 1300 UTC on 22 March, although, none of the meteorological stations detected precipitation at ground level. This indicates that the rain droplets evaporated before reaching the surface.

4 Foehn effect on frontal clouds and solar radiation

As mentioned, on 22 March, the passage of the Cyprus low with its frontal system over Israel towards the Dead Sea valley was accompanied by both significant frontal cloudiness and a large amount of dust pollution, significantly reducing surface solar radiation. To study the foehn-induced effect on clouds and solar radiation in the Dead Sea valley, we analyzed radar data of cloud top height together with pyranometer measurements of surface solar radiation at two sites: the Negba site near the Mediterranean coast and the Dead Sea buoy in the Dead Sea (Fig. 1 and Table 1).

In the morning before 0900 UTC, both radar data and pyranometer measurements of solar radiation showed the absence of clouds over the upwind side of the Judean Mts. and over the Dead Sea. At 0900 UTC, west winds brought significant cloudiness to the upwind side of the Judean Mts. (Fig. 13). Radar showed multilayer clouds characterized by cloud top heights from 1.5 to ~8 km (Fig. 13), although, the clear-sky conditions still remained on the downwind side of the mountain ridge. One hour later clouds of top height from 3 – 4 km covered the Dead Sea, as was clearly seen in radar and pyranometer data at the Dead Sea buoy (Figs. 13 and 14). At 1100 UTC, both the upwind and downwind sides of the Judean Mts. were covered by multilayer clouds of top heights from 1.5 to ~8 km (Fig. 13).

At the Negba monitoring site, in the morning of 22 March before the passage of the Cyprus low, solar radiation increased at the same rate as on the previous day, which was characterized by cloud-free conditions (Fig. 14). The maximum solar radiation of 920

W m^{-2} was observed at 0810 UTC. Then the solar radiation sharply decreased and reached the minimum of 90 W m^{-2} at 1010 UTC. During the following three hours solar radiation in Negba gradually increased and, at 1240 UTC, reached values for clear-sky conditions, as those observed on the previous day (21 March) (Fig. 14).

On 22 March, similarly to solar radiation at Negba, solar radiation at the Dead Sea buoy (under cloud-free conditions) increased gradually up to a maximum of 860 W m^{-2} at 0940 UTC, close to the local noon (Fig. 14). The maximum at the Dead Sea buoy occurred 90 minutes later than at Negba. Then, during the passage of the Cyprus low, solar radiation sharply dropped to 160 W m^{-2} at 1020 UTC, followed by a further gradual decrease to the minimum of 50 W m^{-2} by 1200 UTC. Starting from 1220 UTC, radar data showed a cloud-free band over the top and over the downwind side of the Judean Mts. (Fig. 15). This cloud-free band was caused by the considerable descending airflow on the downwind side of the mountains due to the development of the foehn phenomenon (Fig. 7). At 1300 UTC, when the most significant descending airflow occurred, radar data showed the disappearance of clouds over the western part of the Dead Sea, where the buoy was located (Fig. 15). At the Dead Sea buoy, this disappearance led to a local maximum in solar radiation of up to 340 W m^{-2} at 1300 UTC, based on pyranometer measurements. This measured solar radiation was only half of the radiation measured by the pyranometer for cloud-free conditions on the previous non-dusty day (Fig. 14). Thus, a comparison between radar cloud data and pyranometer measurements of surface solar radiation allowed us to detect the unexpected result that, in the absence of clouds, solar radiation was not able to reach its clear-sky values. This fact can be explained by extreme dust pollution in the Dead Sea valley which significantly contributed to the decrease in surface solar radiation in the valley. Only after 1400 UTC, when the dust AOD decreased, the solar radiation at the Dead Sea buoy reached its clear-sky values, as those observed on the previous day.

6. Conclusions

As mentioned, despite the long history of investigation of foehn phenomena, there are few studies of the influence of foehn winds on air pollution and none in the Dead Sea valley. For the first time the foehn phenomenon and its effects on local dust pollution, frontal cloudiness and surface solar radiation were analyzed in the Dead Sea valley, as it occurred on 22 March 2013. This was carried out using both numerical simulations and observations.

During foehn development both horizontal and vertical wind components significantly increased on the downwind side of the Judean Mountains compared to the winds on the upwind side. The increase in wind speed was accompanied by air heating in the valley and air cooling on the top of the Judean Mts. Weak precipitation over the upwind side of the Judean Mts. was detected by radar measurements. However, the rain droplets evaporated before reaching the ground. In the valley, model data and measurements showed that relative humidity decreased from 40% to 20% when hot foehn winds reached their maximum speed. An ascending airflow was created in the central and eastern Dead Sea valley and a descending airflow in the western Dead Sea valley. Radar data showed a passage of frontal cloudiness through the area of the Dead Sea valley leading to a sharp drop in noon solar radiation (from 860 W m^{-2} to 50 W m^{-2}), based on pyranometer measurements. The strong descending airflow over the downwind side of the Judean Mts. led to the formation of a cloud-free band followed by only the partial recovery of solar radiation because of the extreme dust pollution caused by foehn winds.

All these facts such as strong hot winds with gustiness on the downwind side of the mountain ridge; decrease in relative humidity in the valley; precipitation on the upwind side of the mountain ridge; formation the cloud-free band over the top of the Judean Mts. are indicative of the presence of a foehn phenomenon in the Dead Sea valley.

This foehn phenomenon produced a considerable effect on local dust pollution in the western Dead Sea valley, which was caused by hot strong foehn winds and by foehn-induced pronounced temperature inversion. The foehn winds, accompanied by turbulence, intensified the saltation mechanism of local dust emissions, while the foehn-induced temperature inversion trapped dust particles beneath this inversion. These two factors caused extreme surface dust concentration in the western Dead Sea valley. The dust pollution was transported by west winds eastward, to the central Dead Sea valley, where the speed of these winds sharply decreased. As a result, a large part of the transported dust particles was captured by the ascending airflow contributing to maximum aerosol optical depth (AOD) over the central Dead Sea valley. On the day under study, the maximum surface dust concentration did not coincide with the maximum AOD: this being one of the specific effects of the foehn phenomenon on dust pollution in the Dead Sea valley.

Based on ten years (1992 – 2002) of hourly averaged wind measurements taken at the Dead Sea hydrometeorological buoy, Hecht and Gertman (2003) showed that strong winds greater than 10 m/s consist of less than 1% of the observations: they are far more prevalent in the winter months (when dust activity is low according to total suspended particle (TSP) measurements) than in the summer months. TSP measurements of dust pollution in the Dead Sea valley were performed during the 5-year period from 2011 to 2015. According to these data, the measured extreme dust concentration on March 22, 2013, up to 7000 $\mu g/m^3$ was at least two times higher than the measured maximum dust concentration on other days. All the above information indicates that the foehn phenomenon observed in the Dead Sea valley on March 22, 2013, was a rare but significant event.

References

Callot Y, Marticorena B, Bergametti G (2000) Geomorphologic approach for modelling the surface features of arid environments in a model of dust emissions: application to the Sahara desert. Geodinamica Acta 13(5): 245-270. http://dx.doi.org/10.1016/S0985-3111(00)01044-5

Baldauf M, Seifert A, Förstner J, Majewski D, Raschendorfer M, Reinhardt T (2011) Operational convective-scale numerical weather prediction with the COSMO model: description and sensitivities. Mon Weather Rev 139(12): 3887-3905. doi:http://dx.doi.org/10.1175/MWR-D-10-05013.1

Brinkmann WAR (1971) What is foehn? Weather 26: 230-239. doi: 10.1002/j.1477-8696.1971.tb04200.x

Gohm A, Harnisch F, Vergeiner J, Obleitner F, Schnitzhofer R, Hansel A, Fix A, Neiniger B, Emeis S, Schafer K (2009) Air pollution transport in an Alpine valley: Results from airborne and ground-based observations. Boundary-Layer Meteorol 131: 441–463. doi:10.1007/ s10546-009-9371-9

Kishcha P, Rieger D, Metzger J, Starobinets B, Bangert M, Vogel H, Schaettler U, Corsmeier U, Alpert P, Vogel B (2016) Modeling of a strong dust event in the complex terrain of the Dead Sea valley during the passage of a gust front. Tellus B 68: 29751. http://dx.doi.org/10.3402/tellusb.v68.29751

Li X, Xia X, Wang L, Cai R, Zhao L, Feng Z, Ren Q, Zhao K (2015) The role of foehn in the formation of heavy air pollution events in Urumqi, China. J. Geophys. Res. Atmos., 120: 5371–5384. doi:10.1002/2014JD022778

Marticorena B, Bergametti G, Aumont B, Callot Y, N'doumé C, Legrand M (1997) Modeling the atmospheric dust cycle: 2. Simulation of Saharan dust sources. J. Geophys. Res. Atmos. 102(D4): 4387-4404. doi:10.1029/96JD02964

Marticorena B (2014) Dust production mechanisms. In: Knippertz P, Stuut J-B (eds) Mineral dust. A key player in the Earth system. Springer Science+Business Media, Dordrecht, Netherlands

McGowan HA, Sturman PA, Owens FL (1996) Aeolian dust transport and deposition by foehn winds in an alpine environment, Lake Tekapo, New Zealand. Geomorphology 15(2): 135–146. doi:10.1016/0169-555X(95)00123-M

McGowan H A, Sturman AP, Kossmann M, Zawar-Reza P (2002) Observation of foehn onset in the Southern Alps, New Zealand. Meteorol. Atmos. Phys. 79: 215–230. doi:10.1007/s007030200004

Nkemdirim LC, Leggat K (1978) The effect of chinook weather on urban heat islands and air pollution. Water Air Soil Pollut, 9: 53–67. doi:10.1007/BF00185747

Norte FA (2015) Understanding and Forecasting Zonda Wind (Andean Foehn) in Argentina: A Review. Atmospheric and Climate Sciences 5: 163-193. http://dx.doi.org/10.4236/acs.2015.53012

Richner H, Hachler P (2013) Understanding and forecasting Alpine foehn, in Mountain Weather Research and Forecasting, Monogr. Springer Atmospheric Sciences Series, Chapter 4, pp. 219 – 260, Springer, Netherlands, doi:10.1007/978-94-007-4098-3_4

Vogel B, Hoose C, Vogel H, Kottmeier C (2006) A model of dust transport applied to the Dead Sea area. Meteorologische Zeitschrift 15: 611-624. http://dx.doi.org/10.1127/0941-2948/2006/0168

Vogel B, Vogel H, Bäumer D, Bangert M, Lundgren K, Rinke R, Stanelle T (2009) The comprehensive model system COSMO-ART - Radiative impact of aerosol on the state of the atmosphere on the regional scale. Atmos Chem Phys 9: 8661–8680. doi:10.5194/acp-9-8661-2009

Acknowledgements This study was made with support from the international Virtual Institute DESERVE (Dead Sea Research Venue), funded by the German Helmholtz Association. Special thanks to the Israel Oceanographic and Limnological Research for providing the meteorological data taken at the Dead Sea buoy.

Table 1. Types of measurements and geographical coordinates of the monitoring sites

Monitoring site	Geographical coordinates and elevation (m ASL)	Types of measurements
Bet Dagan	32.01^{o}N; 34.81^{o}E; 31 m	cloud radar
Dead Sea buoy	31.42^{o}N; 35.44^{o}E; -420 m	meteo, pyranometer
Hefez Hayyim	31.79^{o}N; 34.81^{o}E; 80 m	meteo
Jerusalem	31.78^{o}N; 35.22^{o}E; 810 m	meteo
Maale Adumim	31.77^{o}N; 35.30E; 490 m	meteo
Matzukei Dargot	31.59^{o}N; 35.39^{o}E; 20 m	meteo
Nativ Halamed Hay	31.69^{o}N; 34.97^{o}E; 275 m	meteo
Negba	31.66^{o}N; 34.69^{o}E; 90 m	pyranometer
Nizzan	31.73^{o}N; 34.63^{o}E; 30 m	meteo
Rosh Zurim	31.66°N; 35.12°E; 950 m	meteo

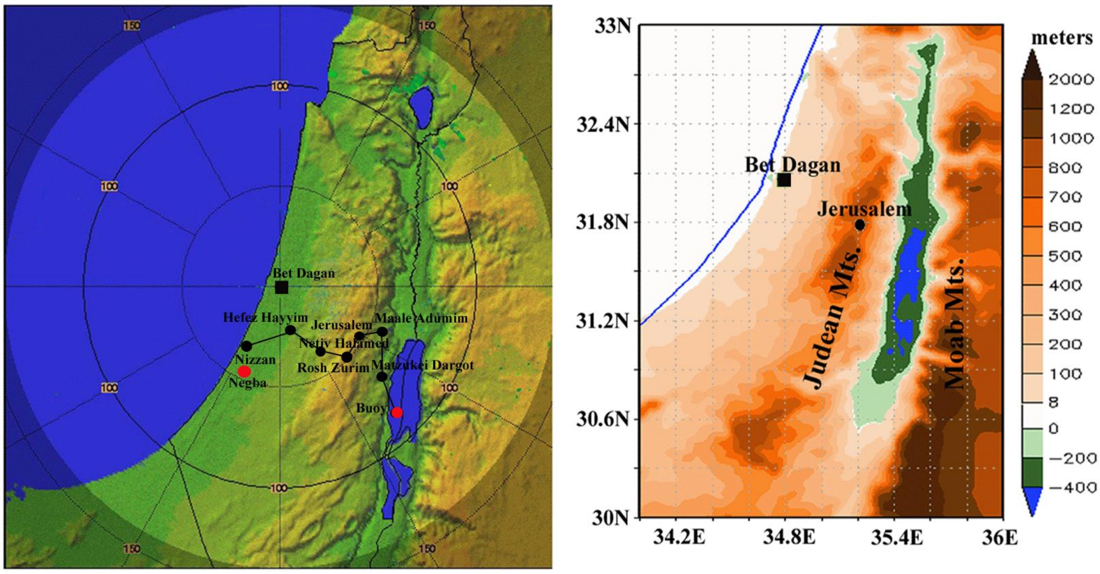

Fig. 1 Geographic (left) and topographic (right) maps of the Dead Sea and surrounding areas. The black circles designate the location of 8 meteorological stations (including the Dead Sea buoy); the red circles designate the location of pyranometers, and the black square designates the radar location.

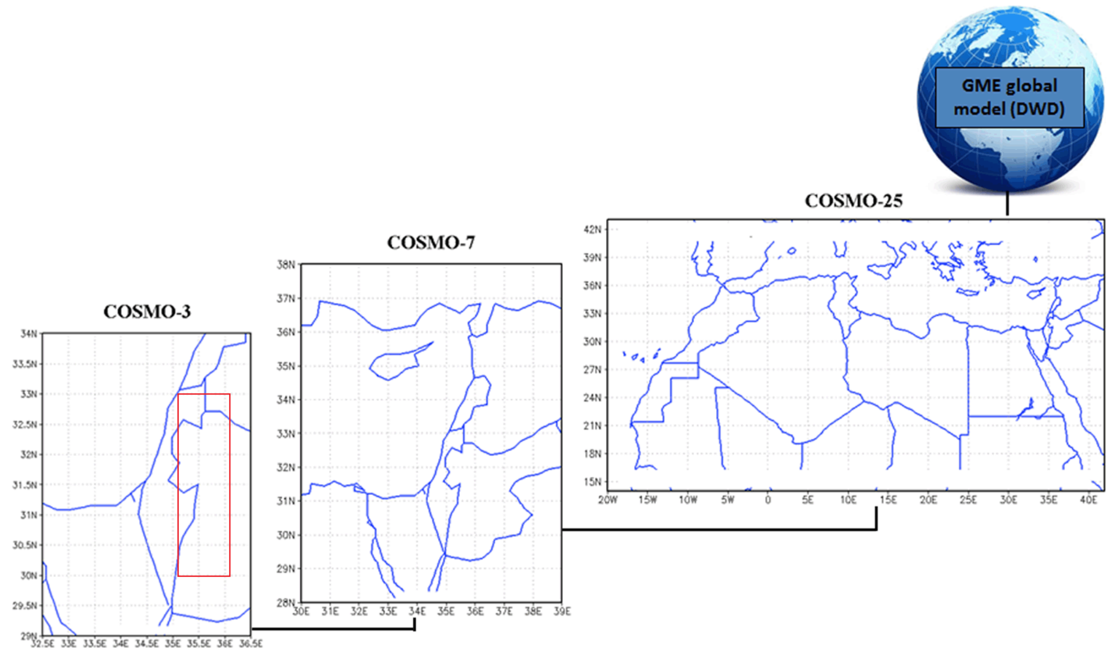

Fig. 2 Large, middle and small model domains. The red box shows the area in which foehn-induced local dust pollution in the area of the Dead Sea valley was simulated.

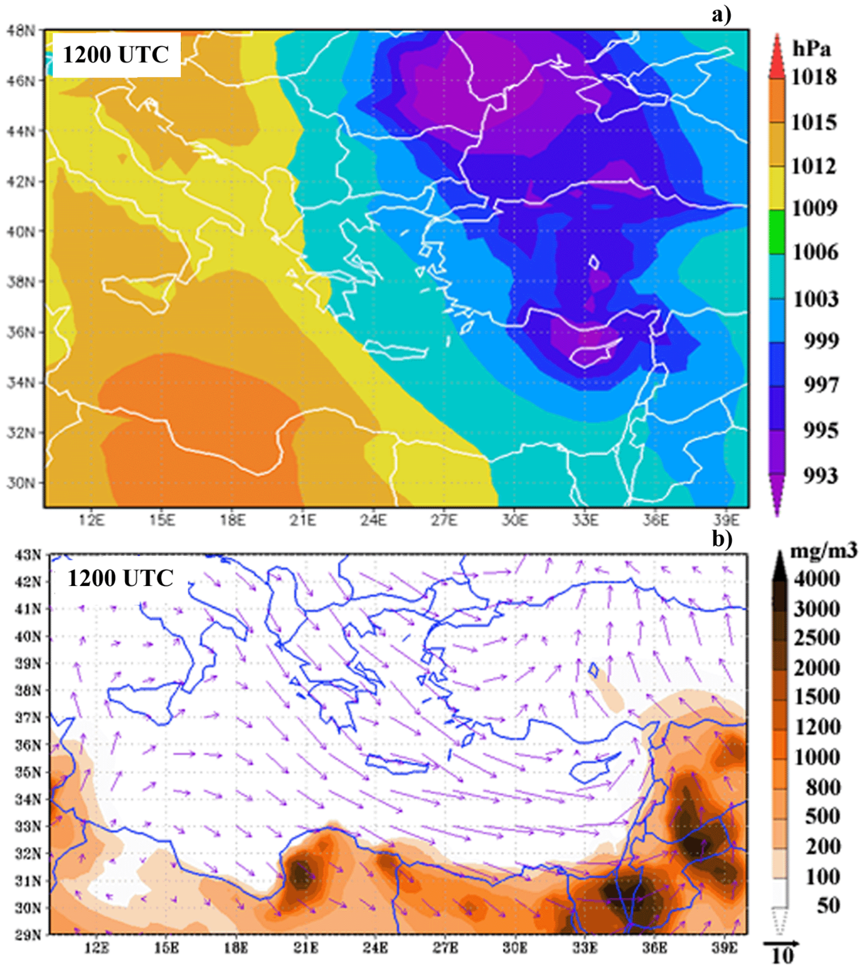

Fig. 3 Maps of (a) sea level pressure on March 22, 2013, at 1200 UTC, based on NASA MERRA reanalysis, and (b) 10-m winds together with surface dust concentration based on DREAM/TAU dust model data.

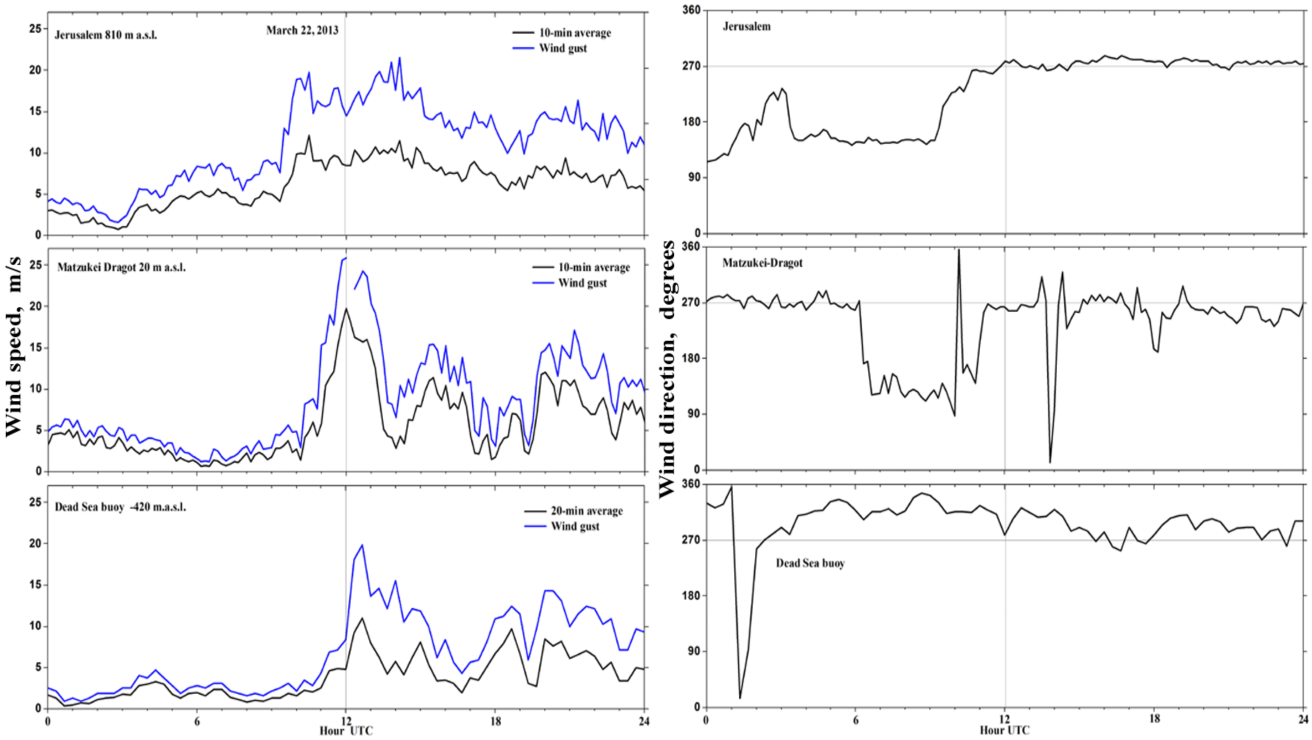

Figure 4. Measurements of surface wind speed and direction at the following three meteorological stations: Jerusalem, Matzukei Dargot and the Dead Sea buoy, on March 22, 2013.

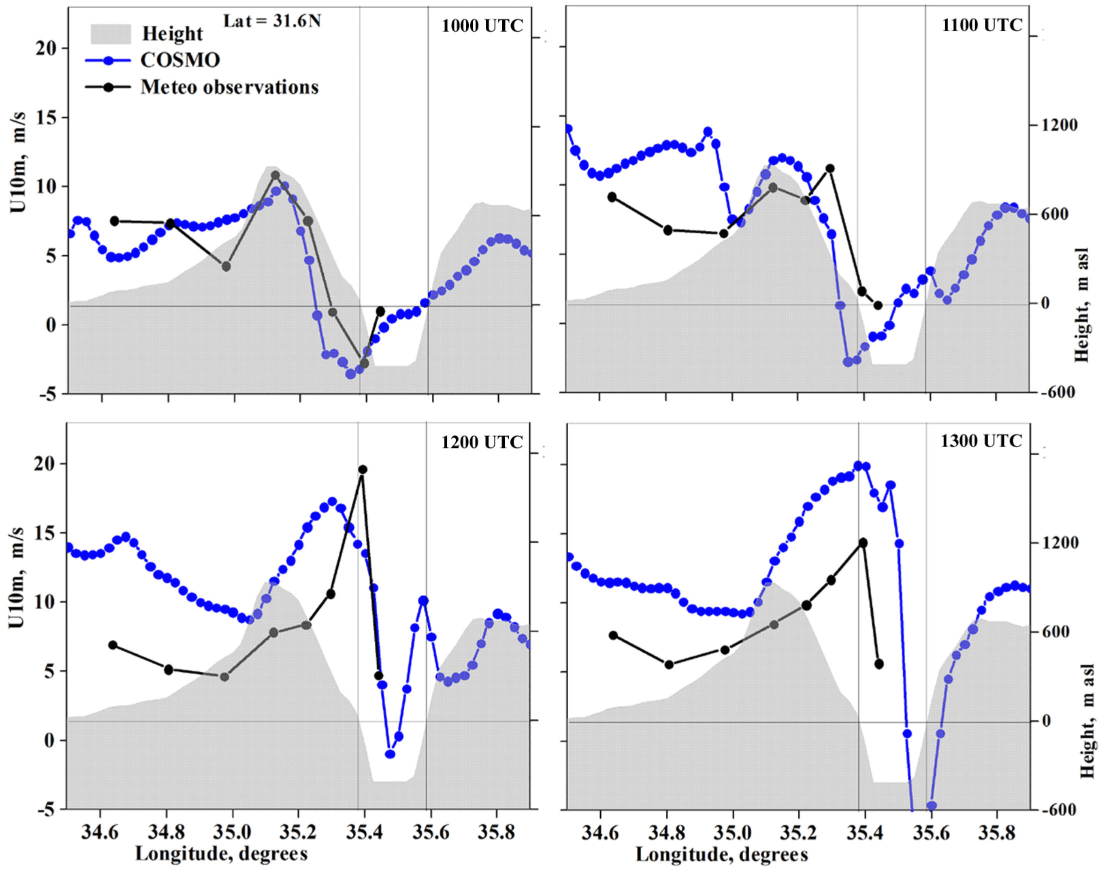

Fig. 5 Measured (black lines) and modeled (blue lines) U-components of near-surface horizontal wind within the west-east cross-section over the Dead Sea valley at 31.6°N. The grey color indicates the model terrain height.

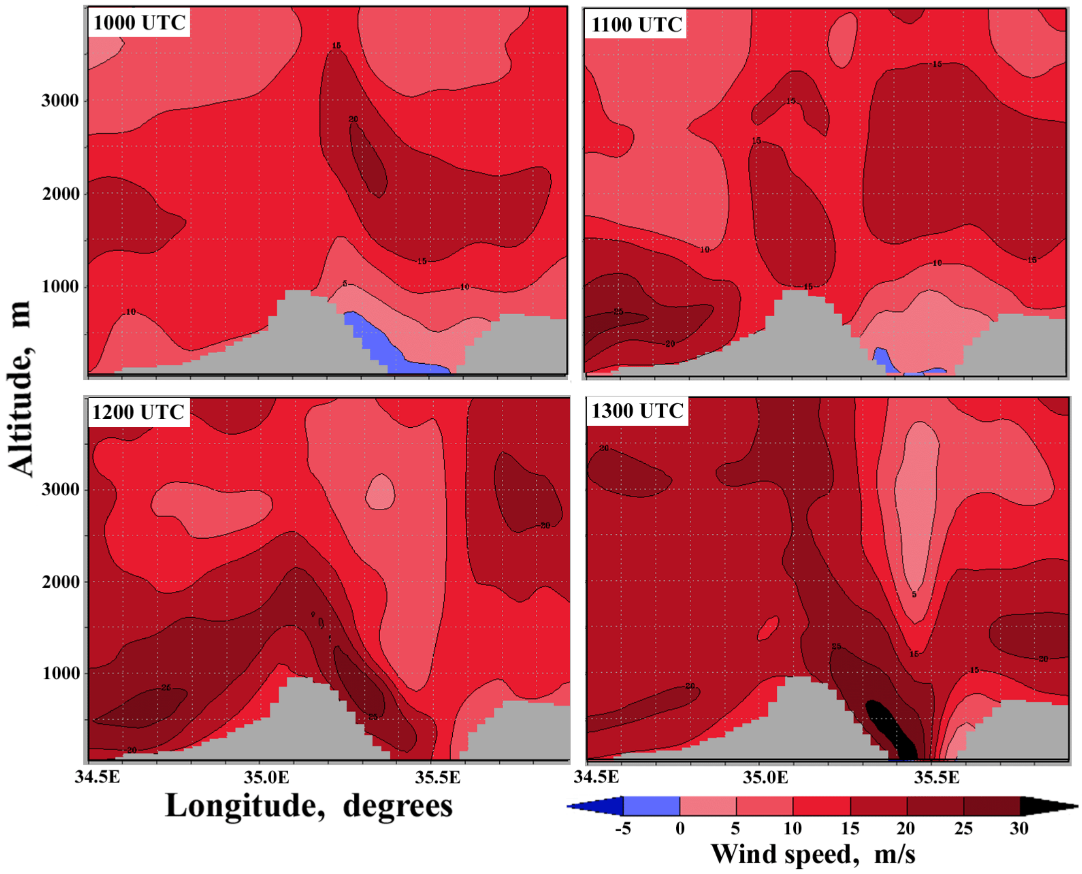

Fig. 6 The vertical distribution of modeled U-component of horizontal wind within the west-east cross-section over the Dead Sea valley at 31.6°N. The model shows very strong winds on the downwind side of the Judean Mts. at 1300 UTC. The grey color indicates the model terrain height.

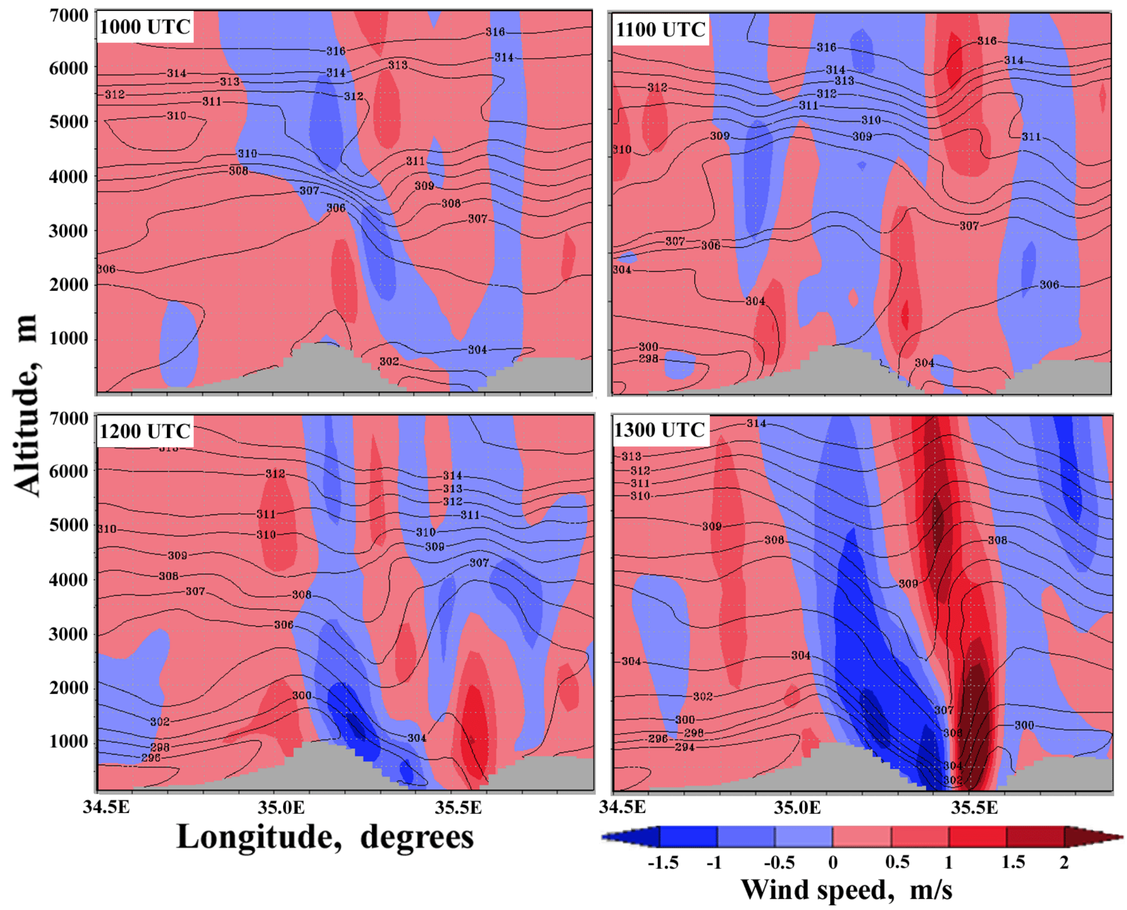

Fig. 7 West-east cross-sections over the Dead Sea valley at 31.6°N of modeled potential temperature (solid lines) and vertical wind speed (colors) from 1000 UTC to 1300 UTC on 22 March 2013. Negative values correspond to a descending airflow while positive values of the vertical velocity correspond to an ascending airflow. The grey color indicates the model terrain height.

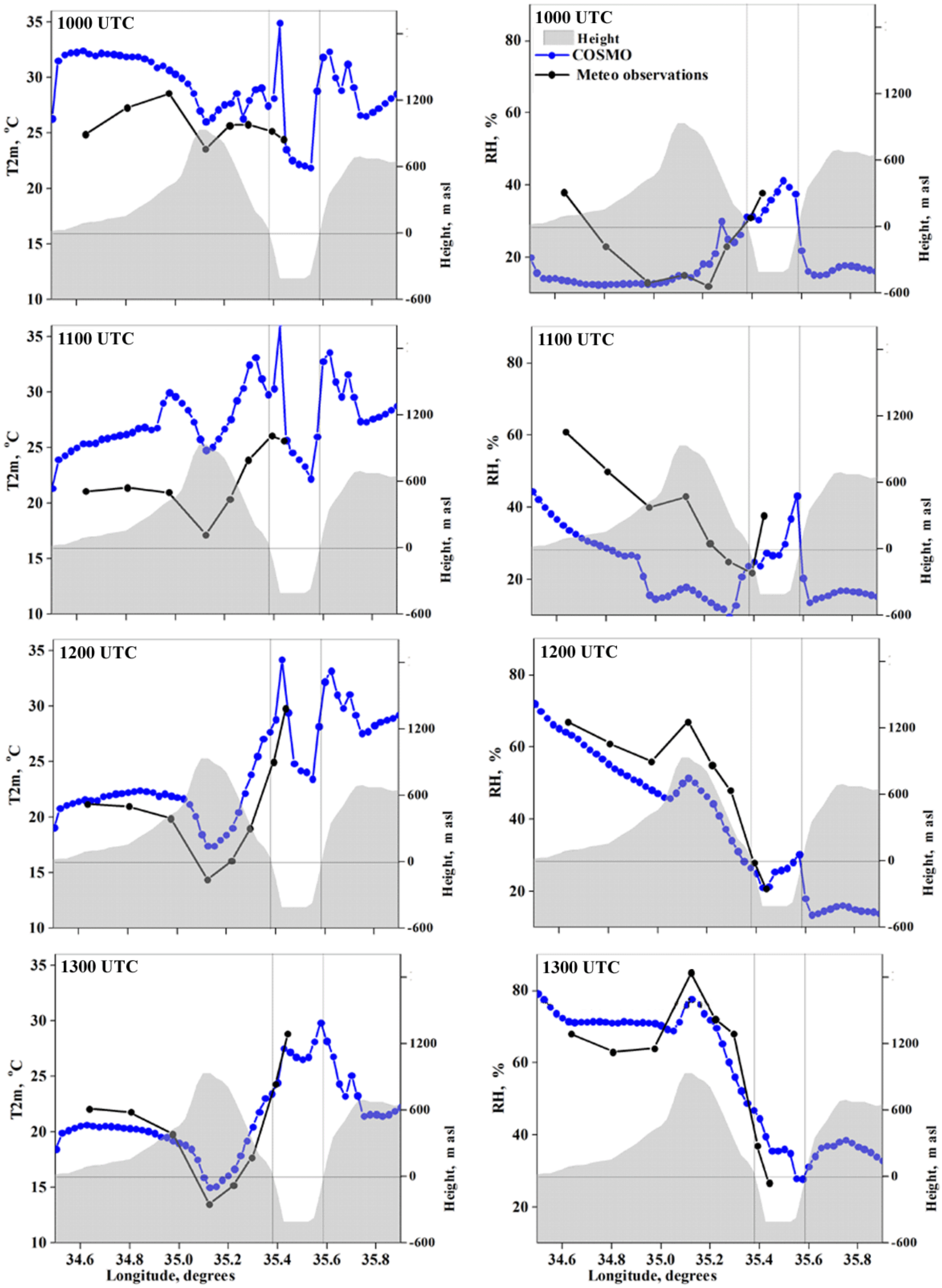

Fig. 8 West-east cross-sections over the Dead Sea valley at 31.6°N of (left panel) measured (black lines) and modeled (blue lines) surface temperature and (right panel) surface relative humidity from 1000 UTC to 1300 UTC on 22 March 2013. The grey color indicates the model terrain height.

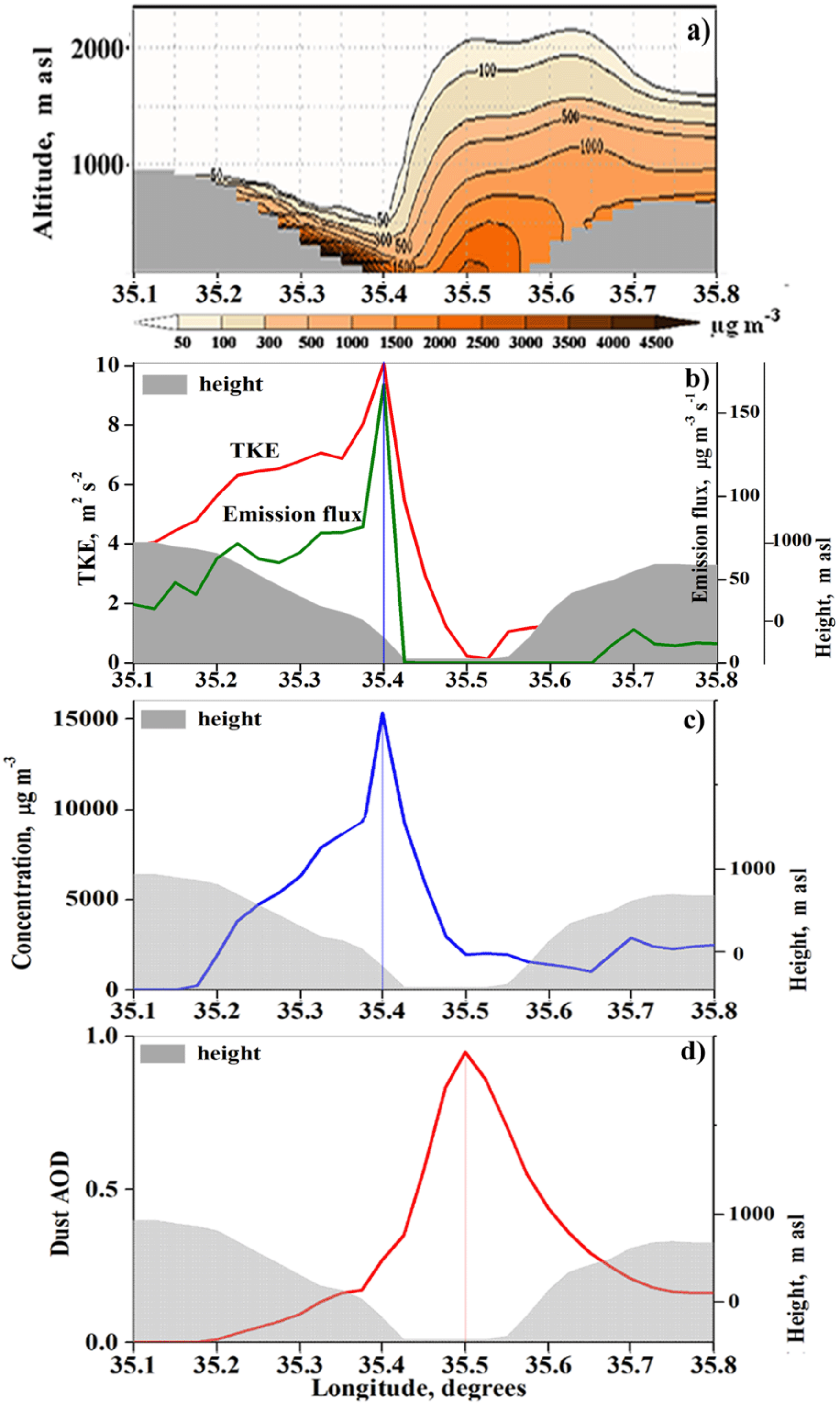

Fig. 9 West-east cross-section over the Dead Sea valley at 31.6°N at 1300 UTC on 22 March 2013 of modeled (a) vertical distribution of dust concentration from local sources; (b) near-surface turbulence kinetic energy (TKE) and emission flux; (c) surface dust concentration; and (d) dust aerosol optical depth (AOD). The vertical blue line designates longitude (35.4°E) of maximum surface dust concentration, while the vertical red line designates longitude (35.5°E) of maximum AOD.

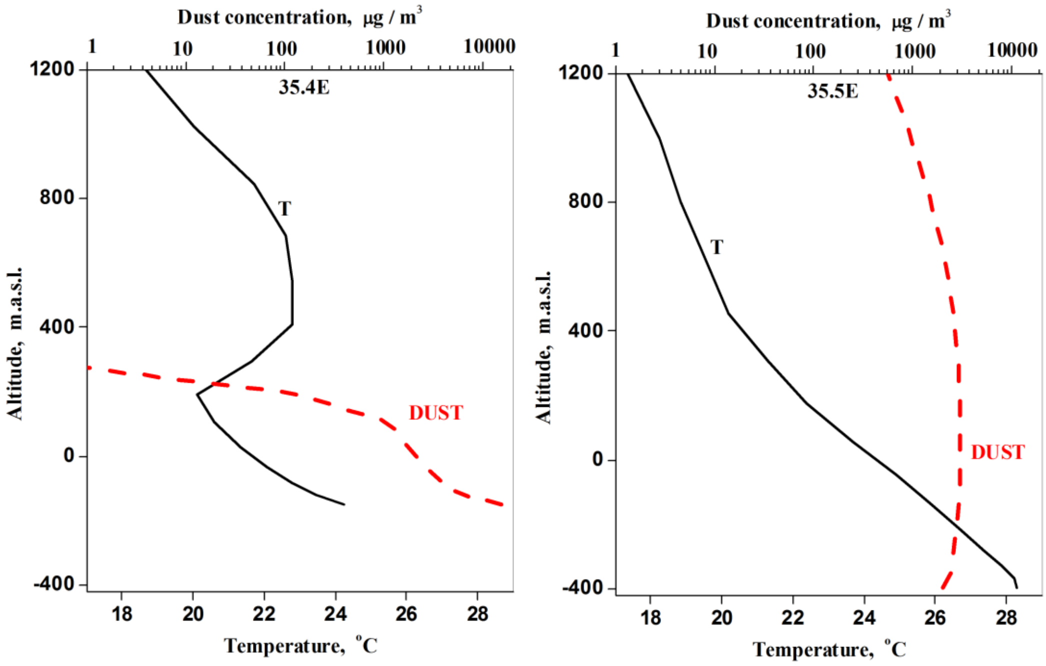

Fig. 10 Modeled vertical profiles of air temperature (T) and dust concentration (DUST) at (a) longitude 35.4°E of maximal surface dust concentration (elevation -157 m) and (b) longitude 35.5°E of maximal dust AOD (elevation -405 m) within the cross-section over the Dead Sea valley at 31.6°N at 1300 UTC on 22 March.

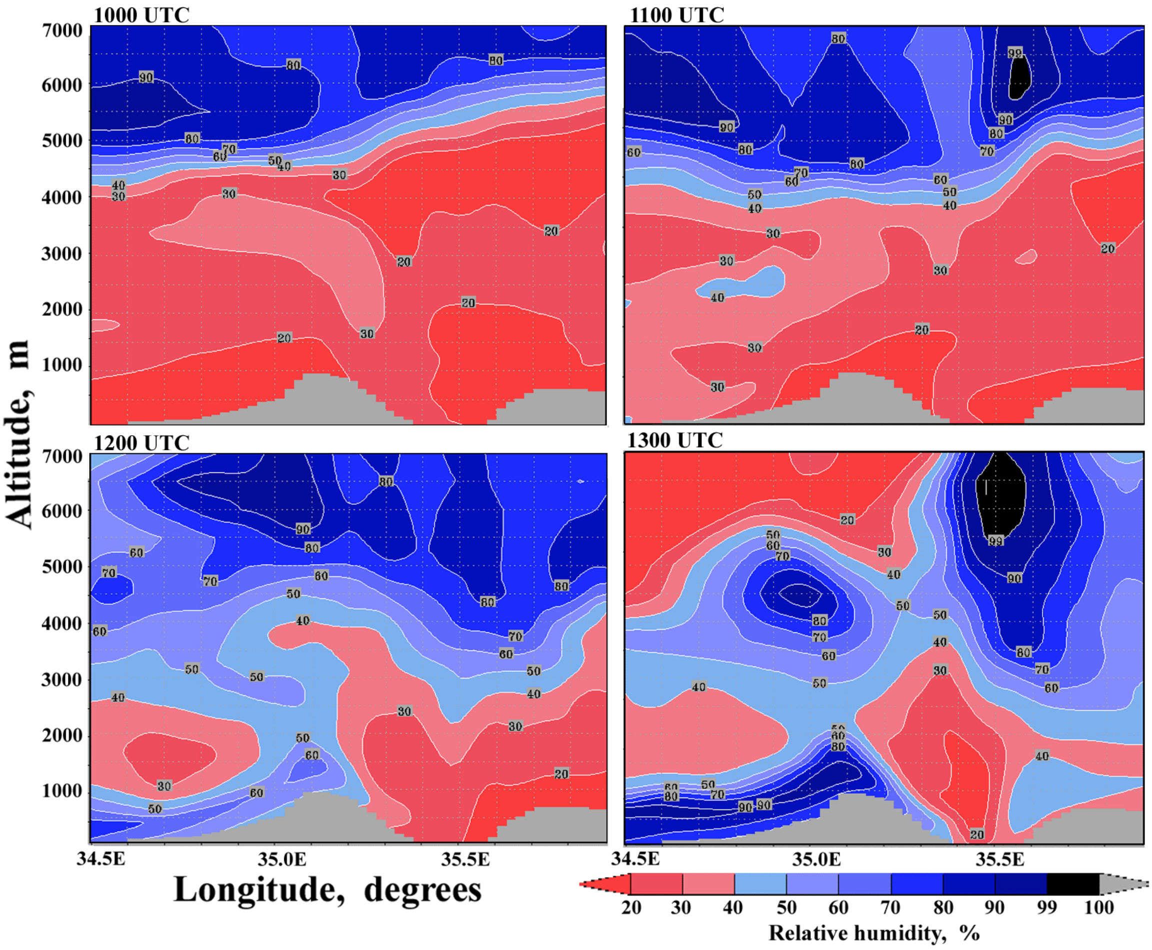

Fig. 11 West-east cross-sections of modeled relative humidity (percentages) over the Dead Sea valley at 31.6^{o}N from 1000 UTC to 1300 UTC on 22 March. The grey color indicates the model terrain height.

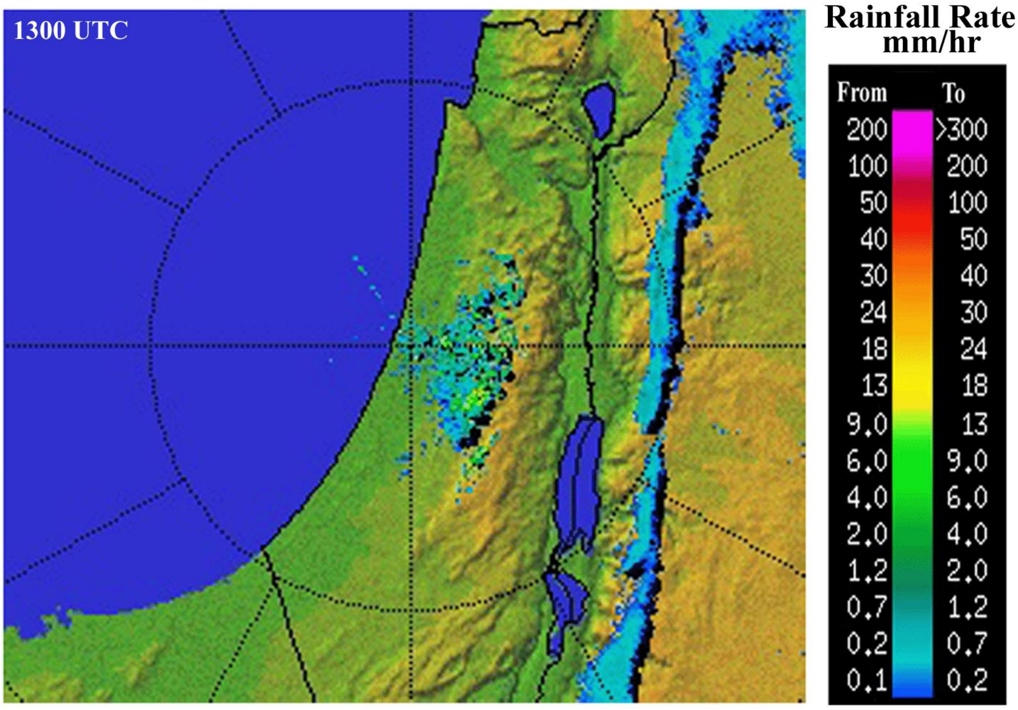

Fig. 12 Radar measurements of rainfall rate at 1300 UTC on 22 March 2013.

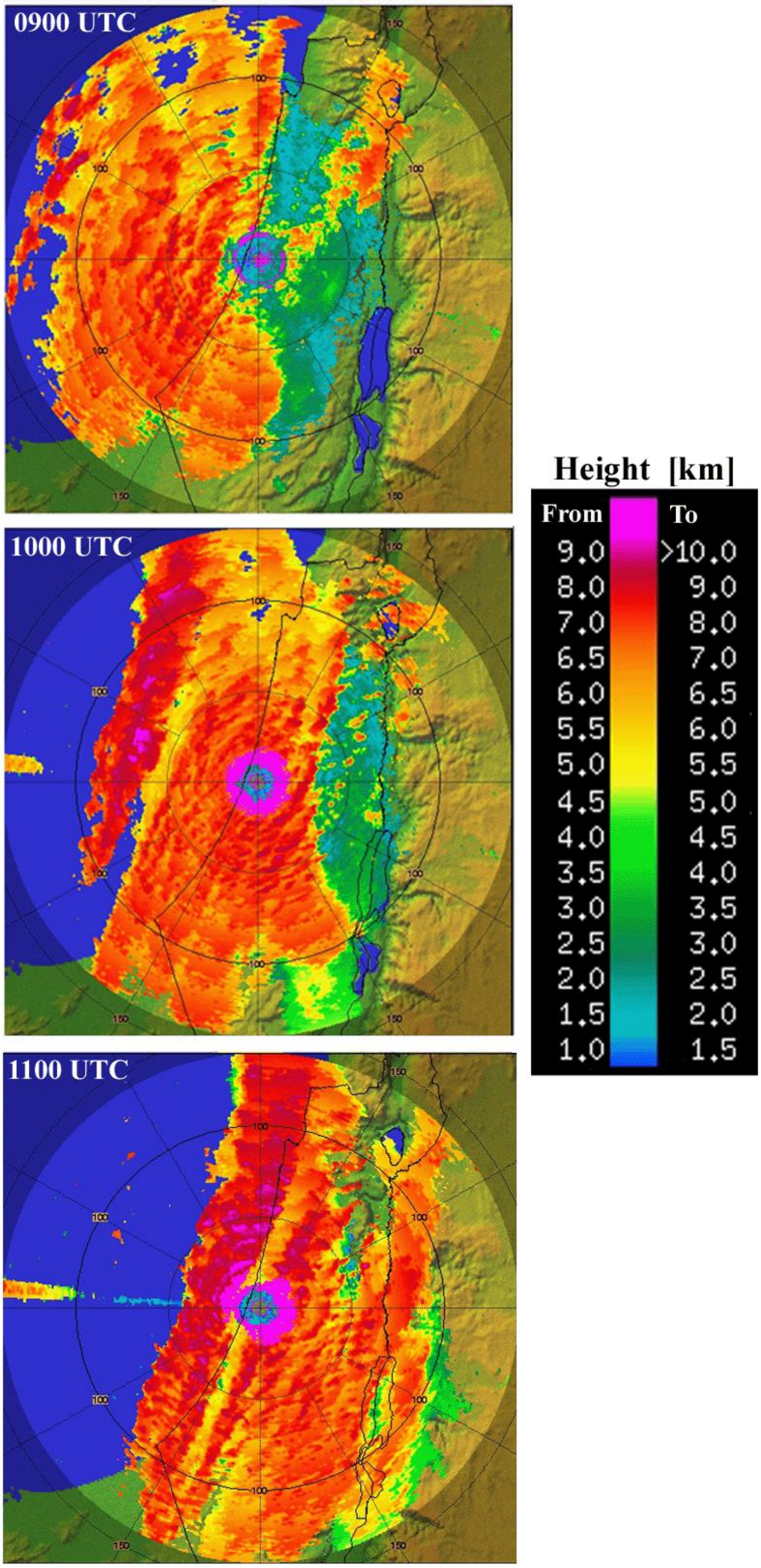

Fig. 13 Radar measurements of cloud top height from 0900 UTC to 1100 UTC on 22 March.

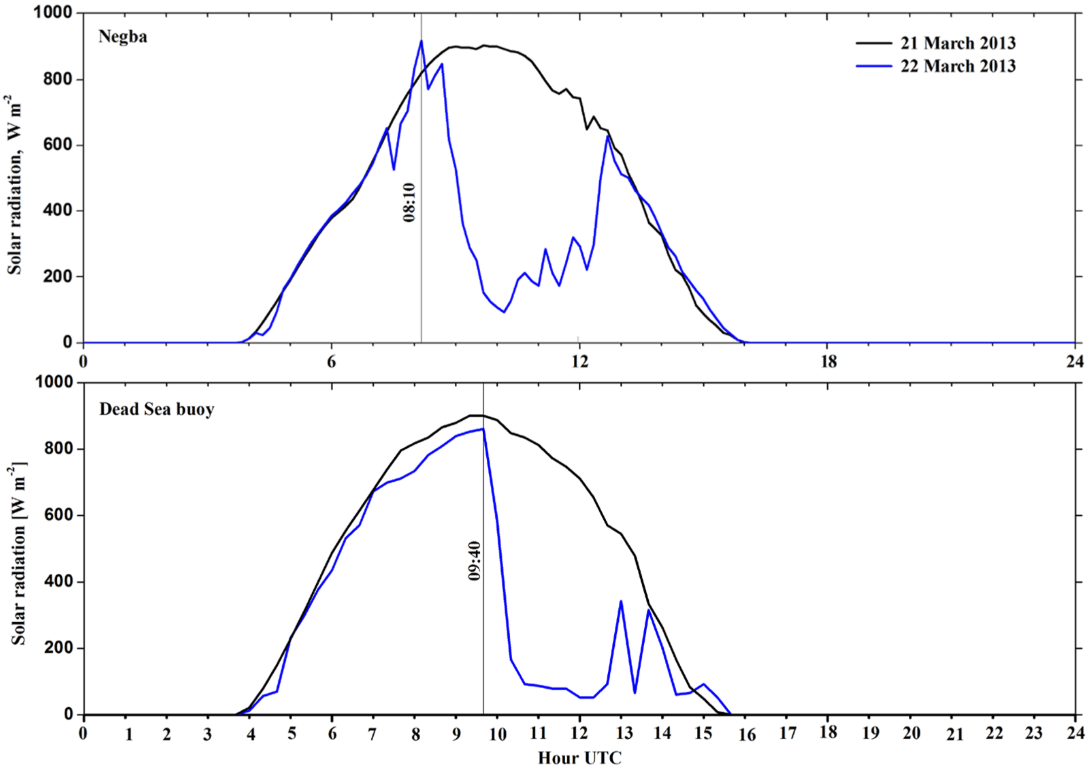

Fig. 14 Measurements of solar radiation on (black lines) 21 March and (blue lines) 22 March 2013 at the Negba monitoring site and at the Dead Sea buoy. The vertical lines designate the specified times (UTC) of maximum solar radiation on 22 March 2013 at the two monitoring sites.

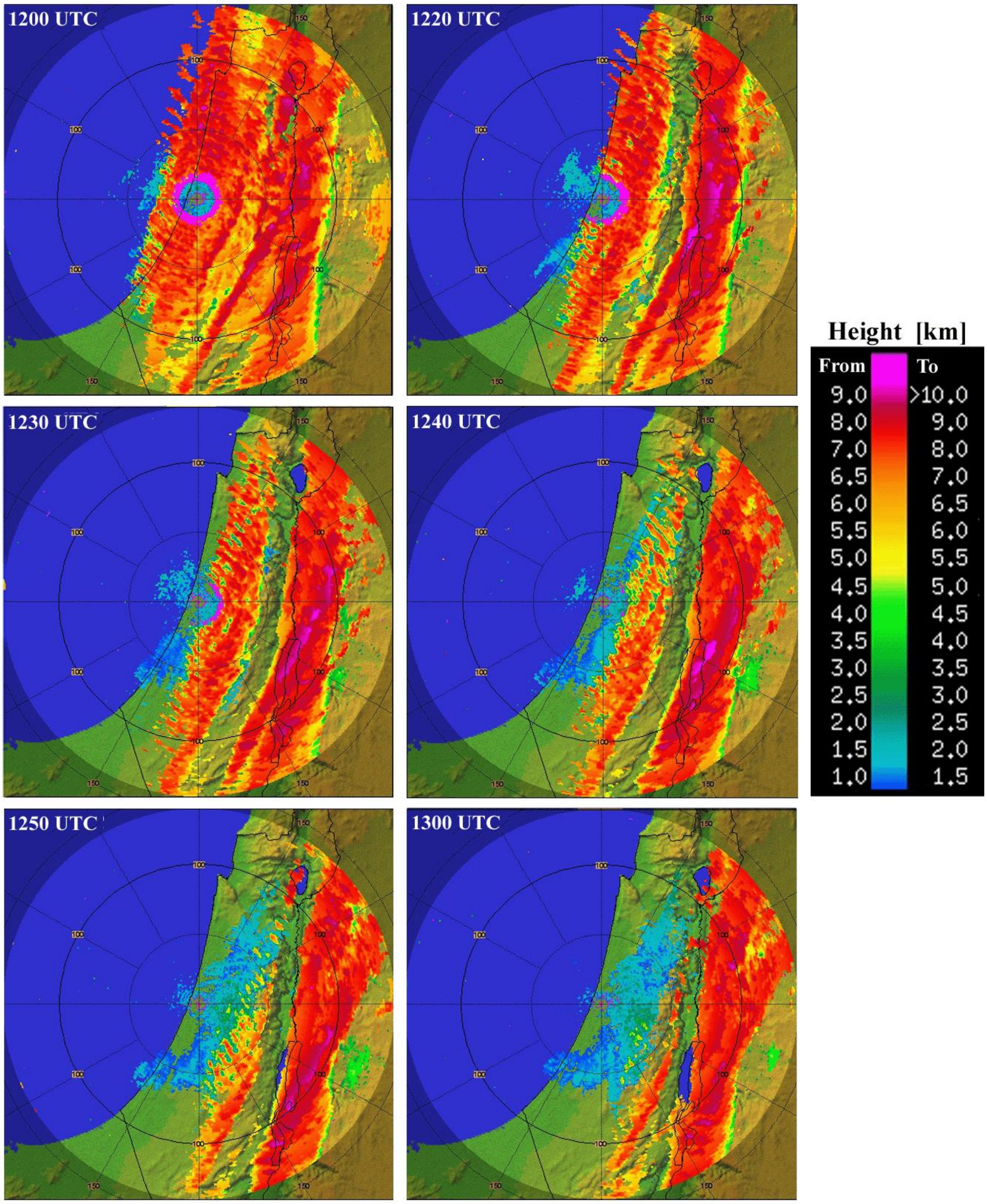

Fig. 15 Radar measurements of cloud top height from 1200 UTC to 1300 UTC on 22 March. A cloud-free band on the downwind side of the Judean Mts. can be clearly seen.